Sensors and Materials, Vol. 35, No. 7 (2023) 2529–2545
MYU Tokyo

S & M 3339

Microwave-cavity-based Online Moisture Sensing for Concrete Fabrication

Kexin Liu,[1,2] Yipeng Zhang,[1,2] Weiguang Wang,[1,3] Xuebin Cheng,[1,4] and Ziyi Weng[5*]

[1]CCCC Second Harbor Engineering Company Ltd., Wuhan 430040, China
[2]Key Laboratory of Large-span Bridge Construction Technology, Beijing 100080, China
[3]Research and Development Center of Transport Industry of Intelligent Manufacturing Technologies of Transport Infrastructure, Beijing 100088, China
[4]CCCC Highway Bridge National Engineering Research Centre Co., Ltd., Beijing 100088, China
[5]Huazhong University of Science and Technology, Wuhan 430074, China

(Received May 15, 2023; accepted July 3, 2023)

Keywords: moisture sensing, microwave cavity, dielectric coefficient

Moisture content is critical to concrete fabrication. Currently, concrete fabrication often involves experienced workers who can gauge whether the water volume is sufficient. This active human involvement requires appearance or thickness checks, which is not suitable for mass production. This method cannot also tell the actual moisture content. Moreover, different workers may give different assessments for the same concrete, which may further lead to different strengths of concrete. Thus, we propose and design a microwave-cavity-based online moisture sensing system to monitor concrete fabrication. Our system utilizes a microwave resonator as a front-end sensor to monitor moisture. This resonator is sensitive to the dielectric coefficient of a particular object. This dielectric coefficient of concrete notably changes when the water yield varies and hence can be readily detected. With this sensitive resonator, we built an online moisture-sensing system. Our prototype achieves moisture sensing with an error of as low as 0.5% and can check moisture content twice a second.

1. Introduction

The precise control of moisture during concrete fabrication is critical to concrete strength. Only when the moisture of concrete reaches a specific level can it be used for construction work. Currently, moisture monitoring is often achieved with the active involvement of experienced workers who can only estimate whether the water volume is sufficient but cannot give a statistical value. Moreover, this method can obtain disruptive results even among experienced workers, as each may provide a different moisture content with the same appearance or thickness of concrete. Therefore, this method often is not suitable for mass production. To the best of our knowledge, most concrete mixers are in the open control state during concrete fabrication, which becomes a bottleneck to their efficiency. With an online moisture-sensing system, the efficiency of concrete fabrication can be significantly improved, saving both energy and time. Thus, we propose and design a microwave-cavity-based[(1–3)] online moisture-sensing system.

*Corresponding author: e-mail: 298494@whut.edu.cn
https://doi.org/10.18494/SAM4504

ISSN 0914-4935

For moisture measurement, there are already some mature moisture sensors on the market, such as the integrated moisture sensor HIH3610. However, the measurement accuracy of these sensors is only as high as 2%. The other method is to use a chemical-physical method for moisture measurement, which is not suitable for solid moisture detection.

Our system is built on the microwave cavity, which is a resonator with an ultrahigh quality (Q) factor.[2,3] The key insight of our system is that this resonator is sensitive to the dielectric coefficient of a particular object. The water or moisture content of concrete is directly linked to the dielectric coefficient. Therefore, by building a sensing system using this microwave resonator as a front-end sensor, we can readily monitor the moisture of concrete. More specifically, when the moisture content of concrete changes, the resonant frequency also changes, which lays the foundation of our online moisture-sensing system. In particular, we use an active signal generator to sweep through this resonator. Then, we use an envelope detector, together with a software-oriented peak detection module, to determine the resonant frequency. By calibrating the resonant frequencies to ground truth moisture, we can thus monitor the moisture online by checking the respective resonant frequency.

This study is novel because of the following achievements:

(1) high-sensitivity moisture sensor design;
(2) high moisture measurement accuracy with an error of as low as 0.5%;
(3) successful application of the moisture sensor to the moisture content measurement of concrete, forming a complete measurement system.

2. Materials and Methods

2.1 System overview

Our system uses a microwave coaxial resonator, a special type of microwave cavity as a front-end sensor for online moisture sensing. During measurement, the concrete under test is in direct contact with this sensor as illustrated in Fig. 1. A dedicated hardware is designed to stimulate and inspect the resonator frequency so as to monitor the moisture. This hardware communicates with a PC through an RS485 interface, enabling remote monitoring. Moreover, the system can perform two humidity checks per second. To start with, we first introduce the detailed design of this resonator.

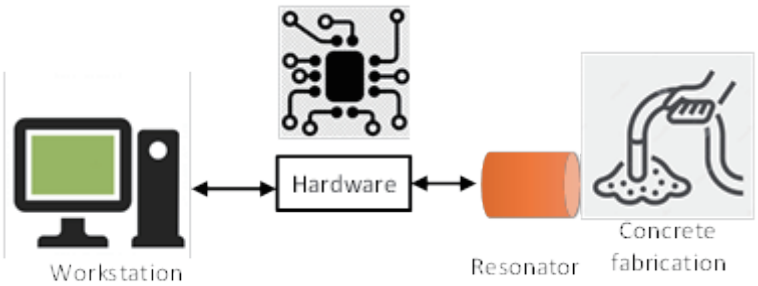

Fig. 1. (Color online) System overview.

2.2 Microwave cavity

2.2.1 Basics on microwave cavity

The microwave coaxial resonator[4,5] is a hollow chamber composed of an inner cylindrical conductor and an outer conductor wall. High-frequency electromagnetic waves will resonate when connected to the inside of the microwave cavity, forming a stable distribution of electromagnetic fields. The coaxial resonator achieves high sensitivity and resolution. When using it as the core component of a sensing system, it is easy to tune and has a robust structure. Owing to their ease of processing and fabrication, coaxial cavity sensors are among the most widely used today. Unlike LCR resonant circuits, the electric and magnetic fields in the coaxial cavity cannot be separated in space, so the electrodynamic equation must be used to solve the electromagnetic model of the coaxial resonant cavity. When the boundary conditions of the outer wall of the coaxial cavity are determined, the conductivity and magnetic permeability of the dielectric in the coaxial cavity become known, and the resonant parameters and electromagnetic field distribution in the cavity can be obtained as well.

The three most practical types of coaxial resonator are as follows:[6–8] $\lambda/4$ coaxial resonators, $\lambda/2$ coaxial resonators, and capacitor-loaded coaxial cavities. Despite their names, these resonators are essentially composed of coaxial lines and cylindrical conductors short-circuited at both ends, with coupling holes at the bottom inserted into the cavity for microwave frequency input and output. Under certain conditions, the electromagnetic wave in the inner conductor will be continuously reflected on the outer wall. Therefore, a standing wave is formed in the coaxial cavity, and the electromagnetic resonance phenomenon occurs. Consequently, the frequency output through the coupling structure is the resonant frequency of the coaxial cavity. Once the volume fraction of each component of the uniformly filled medium in the coaxial cavity changes, the dielectric properties also change. Correspondingly, the electromagnetic field between the inner and outer conductors will cause a small disturbance due to the change in the type of medium used, which in turn causes a change in resonant frequency. The resolution of microwave frequencies can reach more than 10^{-7} Hz, so coaxial cavity sensors have high accuracy for non-charge detection. For concrete, when the structure of the coaxial resonator and the temperature of concrete are determined, a change in concrete moisture content will cause a change in dielectric coefficient in the resonator At the same time, this moisture change can cause the offset of the resonant frequency of the coaxial cavity. Therefore, the moisture content of concrete can be indirectly determined by measuring the resonant frequency of the coaxial cavity sensor.

According to their structural characteristics, microwave resonators mainly include rectangular, cylindrical, and coaxial resonators, and each type of resonator has its own electromagnetic field distribution mode. As a commonly used sensor type in the field of dielectric characteristic analysis, the main mode of guided waves in the coaxial resonant cavity is the transverse electromagnetic mode (TEM).[9,10] The advantage of this specific mode is that the electromagnetic field structure inside the cavity is simple and stable, without the limitation of dispersion and low frequency. As a result, such coaxial cavity sensors are widely used to

measure the fractional microconcentration of materials. Figure 2 shows the electromagnetic field structure diagram of TEM in the coaxial resonator.

When the coaxial resonator is in this mode, $E_Z = 0$, $H_Z = 0$ in the axial direction. The electric and magnetic field distributions between the inner and outer conductors conform to the following equation:[10]

$$\begin{cases} \nabla_t^2 E(\gamma,\varphi) = 0, \\ \nabla_t^2 H(\gamma,\varphi) = 0. \end{cases} \tag{1}$$

Assuming that the outer wall surface of the coaxial resonator is the ideal conductor boundary condition, and the TEM electromagnetic wave in the cavity has been in a simple harmonic vibration state, the electromagnetic field distribution of the resonator is equivalent to the static field distribution on the section perpendicular to the coaxial line. At this time, the electromagnetic field of TEM only has $E\gamma$ and $H\varphi$ components. Let a be the radius of the cylindrical inner conductor, and electromagnetic waves propagate in the positive direction of the z-axis; we can thus obtain:[7]

$$\begin{cases} E_r = \dfrac{E_0 a}{r} e^{-j\beta z}, \\ H_\varphi = \dfrac{H_0 a}{\eta r} e^{-j\beta z}. \end{cases} \tag{2}$$

where r is the length of the coaxial line from the center, $\eta = \sqrt{\mu/\varepsilon}$, $\beta = \omega\sqrt{\mu\varepsilon}$, ω is the angular frequency, and μ is the conductivity.

2.2.2 Main parameters of microwave cavity

2.2.2.1 Resonant frequency

The resonant frequency refers to the frequency at which the electric field strength in a particular mode in the resonator reaches its maximum, that is, the frequency at which simple

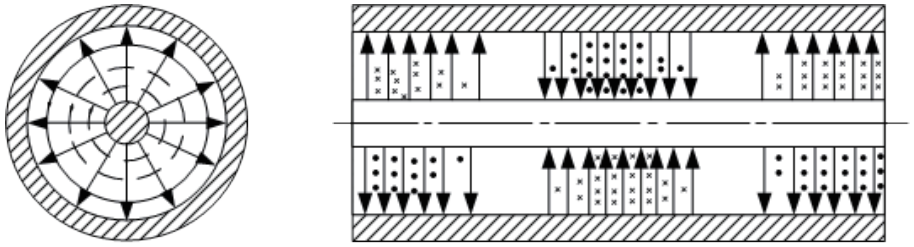

(a) (b)

Fig. 2. Field structure diagram of TEM in coaxial cavity. (a) Cross-sectional and (b) longitudinal views.

harmonic vibrations occur in that mode. The resonant frequency can represent the oscillation state of electromagnetic waves in the coaxial resonant cavity and can also give the prerequisite for resonance in the cavity, that is, the frequency selection characteristics of the coaxial resonator. The guide wave equation of the coaxial resonant cavity is solved to obtain the expression of the guided wave:[11,12]

$$k^2 = k_u^2 + k_v^2 + k_z^2 = \beta^2 + k_c^2, \tag{3}$$

where k represents the wavenumber of the guided wave; k_u, k_v, and k_z represent the components of k in different directions in three dimensions; β represents the phase shift constant; k_c stands for the cut-off wavenumber.

Under radiation boundary conditions, electromagnetic waves can propagate without limit, and no loss occurs. Therefore, electromagnetic waves are horizontal standing and vertical (z-directional) traveling waves of unrestricted navigation systems, and k_c and β are their characteristic parameters. Since the cut-off wavenumber k_c is a discrete quantity and the phase shift constant β is a continuous quantity, it is proved that the wavenumber k, that is, the frequency, is a continuously variable quantity, indicating that the electromagnetic wave has no resonant characteristics in the vertical direction.[7–9]

2.2.2.2 *Q* factor

The resonant frequency gives the frequency selection characteristics of the coaxial resonator. The frequency selection ability of a coaxial resonator varies with its size. This ability can be quantitatively assessed using an important parameter, the Q factor. The Q factor can visually characterize the frequency selection capacity of the coaxial resonator, which is defined as the ratio of the total energy in the resonator to the energy loss in a single cycle when the electromagnetic wave reaches a stable simple harmonic vibration state, representing the energy storage capacity of the resonator. The Q factor is defined using the following formula:[13,14]

$$Q_0 = 2\pi \frac{W}{W_T} = \omega_0 \frac{W}{P_L}, \tag{4}$$

where W is the total energy in the coaxial cavity, W_T is the energy loss in a single cycle within the cavity, and P_L is the lost power in the cavity. W and P_L can be solved using the following formulas:[13]

$$W = W_e + W_m = \frac{1}{2}\int_V \mu |H|^2 dV = \frac{1}{2}\int_V \varepsilon |E|^2 dV, \tag{5}$$

$$P_L = \frac{1}{2}\oint_S |J_S|^2 R_S dS = \frac{1}{2} R_S \int_S |H_t|^2 dS, \tag{6}$$

where R_S is the surface resistance of the conductor, which becomes the main cause of energy

loss; H_t is the tangential magnetic field on the inner wall of the conductor, while $J_S = n \times H_t$, where n is the normal vector. Then,

$$Q_0 = \frac{\omega_0 \mu}{R_S} \frac{\int_V |H|^2 \, dV}{\int_S |H_t|^2 \, dS} = \frac{2}{\delta} \frac{\int_V |H|^2 \, dV}{\int_S |H_t|^2 \, dS}, \tag{7}$$

where δ is the depth of the inner wall of the conductor:

$$\delta = \frac{2R_S}{\omega_0 \mu} = \sqrt{\frac{2}{\omega_0 \mu \sigma}}. \tag{8}$$

The above formulas are used to deduce Q theoretically, from which one can inspect its properties. In practice, Q can be visually inspected using the S parameter, namely, $S21$ or $S12$. The sharper the peak in the S parameter, the higher the Q.

2.2.3 $\lambda/4$ microwave coaxial resonator design

In our design, we chose the $\lambda/4$ microwave coaxial resonator[15–17] as our front-end sensor. The structure of this coaxial resonator is shown in Fig. 3. This coaxial resonator can essentially be seen as a section of a coaxial line that is open at one end and short-circuited by a metal conductor at the other end. To facilitate the calculation, we denote the diameter of the inner conductor of the coaxial cavity as $d = 2a$ and the inner diameter of the outer wall conductor as $D = 2b$.

If the electromagnetic wave signal enters, a traveling wave in a simple harmonic vibration state will be formed inside the $\lambda/4$ coaxial cavity and a circular waveguide with a certain cut-off range will be formed at the open end. Owing to the different boundary conditions of the two ends of the $\lambda/4$ coaxial cavity, when electromagnetic waves resonate in the cavity, the cavity length l is equal to an odd number of times of 1/4 wavelength λ_0:

$$l = \left[(2p-1)\lambda_0 \right] / 4, (p = 1,2,3,...). \tag{9}$$

Therefore, the resonant wavelength λ_0 of the $\lambda/4$ coaxial cavity is[15]

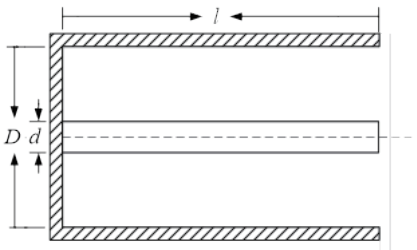

Fig. 3. Structure of $\lambda/4$ microwave coaxial resonator.

$$\lambda_0 = \frac{4l}{2p-1}, \tag{10}$$

and the respective Q_0 factor is

$$Q_0 = \frac{\lambda_0}{\delta} \cdot \frac{1}{4 + \frac{l}{D}\frac{1+(D/d)}{\ln(D/d)}}. \tag{11}$$

From the above equation, it can be concluded that when the cavity length l is constant, each p value corresponds to a resonant wavelength λ_0. This indicates that there are many resonant wavelengths λ_0 when the electromagnetic wave in the $\lambda/4$ coaxial cavity resonates, which reveals the polyharmonics of the coaxial resonator. At the same time, when the resonant wavelength is constant, the resonant frequency f_0 of the coaxial cavity is also determined, and there will be multiple l values corresponding to it.

When designing the overall size of the $\lambda/4$ coaxial cavity, in addition to determining l, the inner and outer conductor diameters, d and D, respectively, should meet the following requirements: First, to ensure the stable existence of the TEM required for the design in the coaxial resonant cavity, other messy modes should not be formed, the circular waveguide at the open end of the $\lambda/4$ coaxial cavity should be in the cut-off state, and the relationship between the inner and outer conductor diameters and the wavelength must be satisfied, i.e., $\pi(a+b) < \lambda_0 \min$. Second, to ensure that the Q of the coaxial resonator is as high as possible, $2 \leq (D/d) \leq 6$.

2.2.4 Resonant frequency as a function of concrete moisture

In this section, we introduce the theoretical relationship between the resonant frequency of the microwave cavity and the concrete moisture.

The wavelengths of electromagnetic waves differ in different media. According to Maxwell's classical electromagnetic theory,[18] wavelength and dielectric refractive index are related; the smaller the refractive index, the longer the wavelength. The following is the wavelength formula after the electromagnetic wave passes through the medium:

$$\lambda = n\lambda_0, \tag{12}$$

where λ_0 is the wavelength of the electromagnetic wave in unlimited space and n is the refractive index of the medium.

Typically, an external electromagnetic field on a polar dielectric causes free and polarized charges in the medium, followed by conduction, polarization, and magnetization currents. For the insulating medium mainly studied in this paper, the free charge and conduction current in the insulating medium are 0 regardless of the frequency of the electromagnetic field applied. Assuming that this homogeneous insulating medium is infinite, the constitutive relation of the electromagnetic properties of the dielectric is[18]

$$\begin{cases} D = \varepsilon_0 E, \\ B = \mu_0 H, \end{cases} \tag{13}$$

where D is the vector displacement of the electromagnetic wave, E is the electric field strength, B is the magnetic induction vector, H is the magnetic field strength, μ_0 is the vacuum permeability, and ε_0 is the vacuum permittivity. According to Maxwell's equations[19,20] of the dielectric, the above constitutive equation can be changed to

$$\begin{cases} \nabla \cdot E = 0, \\ \nabla \times E = -\dfrac{\partial B}{\partial t}, \end{cases} \tag{14}$$

$$\begin{cases} \nabla \cdot B = 0, \\ \nabla \times B = \mu_0 j + \mu_0 \varepsilon_0 \dfrac{\partial E}{\partial t}. \end{cases} \tag{15}$$

Thus, the wave equation of planar electromagnetic waves in a homogeneous insulating medium is obtained as

$$\frac{\partial^2 E}{\partial t^2} = \frac{1}{\varepsilon\mu} \nabla^2 E, \tag{16}$$

$$\frac{\partial^2 H}{\partial t^2} = \frac{1}{\varepsilon\mu} \nabla^2 H. \tag{17}$$

Solving the above equation yields the wave velocity of electromagnetic waves in a homogeneous insulating medium:

$$v = \frac{1}{\sqrt{\varepsilon\mu}}. \tag{18}$$

According to the relationship between the speed of light and the refractive index in Maxwell's medium theory,[19–22] Eq. (18) can be converted to the relationship between the dielectric constant and the dielectric refractive index:

$$v = \frac{1}{\sqrt{\varepsilon\mu}} = \frac{1}{\sqrt{\varepsilon_0\mu_0}} \cdot \frac{1}{\sqrt{\varepsilon_r\mu_r}} = \frac{c}{\sqrt{\varepsilon_r\mu_r}} = \frac{c}{n}, \tag{19}$$

where c is the wave velocity in a vacuum (that is, the speed of light), μ is the magnetic permeability of the medium ($\mu = \mu_r * \mu_0$), ε is the dielectric constant of the medium ($\varepsilon = \varepsilon_r * \varepsilon_0$), μ_r is the relative permeability of the medium, and ε_r is the relative permittivity of the medium.

From the above equation, it is nontrivial to deduce that $n = \sqrt{\varepsilon_r \mu_r}$. Combined this with the fact that the dielectric medium of inorganic materials such as sand and gravel is $\mu_r \approx 1$,

$$n = \sqrt{\varepsilon_r}. \tag{20}$$

The above equation shows that the refractive index of a medium is only a function of its relative permittivity. In general, to facilitate research and calculation, we only consider the relative permittivity of dielectric materials. Therefore, adding Eq. (20) into Eq. (12), we can obtain

$$\lambda = \sqrt{\varepsilon}\lambda_0. \tag{21}$$

Combining the formula $\lambda_f = c$ for frequency and wavelength gives the following relationship between dielectric constant and frequency:

$$\varepsilon = \frac{c^2}{f^2 {\lambda_0}^2}. \tag{22}$$

At this time, the theoretical calculation formula for the moisture content of the three coaxial resonators in the microwave frequency band can be obtained as

$$\varepsilon = \frac{c^2 (2p-1)^2}{16 l^2 f^2} \ (p = 1,2,3\ldots), \tag{23}$$

$$\varphi = \frac{\left[\frac{c^2 (2p-1)^2}{16 l^2 f^2} - \varepsilon'_o\right]\left[\left(\varepsilon'_\alpha + 4\right)^2 + {\varepsilon''_\alpha}^2\right]}{3\varepsilon'_o\left[\left(\varepsilon'_\alpha - 2\right)\left(\varepsilon'_\alpha + 4\right) - {\varepsilon''_\alpha}^2\right]}. \tag{24}$$

The above equation lays the foundation of our online moisture monitoring system. It is observable that the volume fraction of water in concrete is related to the temperature, dielectric properties, and structure of the coaxial resonator of the sand and gravel mixture. When the structure of the coaxial cavity is determined, the resonant frequency f of the coaxial cavity and the temperature of the sand and gravel mixture can be measured to determine the moisture content in concrete.

On the basis of the above theoretical analysis, we can see that the higher the resonant frequency, the higher the sensitivity of the resonator in sensing dielectric variations. Therefore, to improve the resolution of moisture sensing, we should configure the resonator with a high resonant frequency. However, when operating at high frequencies, such as 10 GHZ, the system's hardware requirements are expected to be significantly higher. Moreover, the complexity increase in hardware can also lead to the instability of a designed hardware circuit, as well as an

increase in its cost. Consequently, for the tradeoff among sensitivity, cost, and complexity, we configured the resonant frequency to around 3 GHz. This configuration leads to l = 70 mm, d = 10 mm, and D = 62 mm. We chose a copper material for our resonator.

2.3 Hardware design

In this section, we present the hardware design. The equivalent circuit of this resonator can be regarded as an LCR harmonic circuit. To determine its resonant frequency, we need an active signal generator. To this end, we use the radio frequency chip ADF4351 to generate different sweeping frequencies to inspect the resonant frequency. Moreover, we leverage AD8317, at up to 10 GHz envelope detector, with a software-oriented peak detector module to search for the resonant frequency. This AD8317 can output the respective envelope in a DC format and we thus use a high-precision ADC, ADS1115, to sample this envelope information. These modules are powered by the voltage stabilizer MIC39100.

All these modules are controlled by a STM32 microcontroller. Moreover, the measurement results, including the resonant frequency, can be uploaded to a PC via an RS485 interface. As the microwave cavity is subject to temperature variations, we thus use the temperature sensor DS18B20 to monitor the surrounding temperature and correspondingly perform compensation. We specifically add the flash memory unit W25Q128 to our system. This memory unit is used for storing measurement results, system fault information, and calibration information. The overall system architecture and system development board are shown in Figs. 4 and 5, respectively.

2.4 Software design

In this section, we present the software design of our system, the diagram of which is shown in Fig. 6. Our software runs on top of FreeRTOS. There are two major concurrent threads at the initial setup. The first one is a thread that is in charge of resetting the hardware if system faults are encountered. This is achieved by the onboard watchdog of STM32. We hence allocate a thread to periodically feed this watchdog. The second one takes charge of the moisture sensing. This second thread first performs a hardware check. This is achieved by reading the specific registers of those hardware modules, including DS18B20, ADS1115, AD8317, ADF4351, and W25Q128.

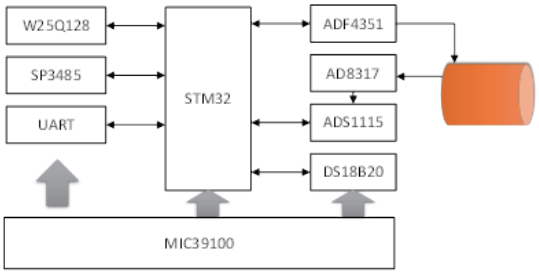

Fig. 4. (Color online) Overall system architecture.

Fig. 5. (Color online) System development board.

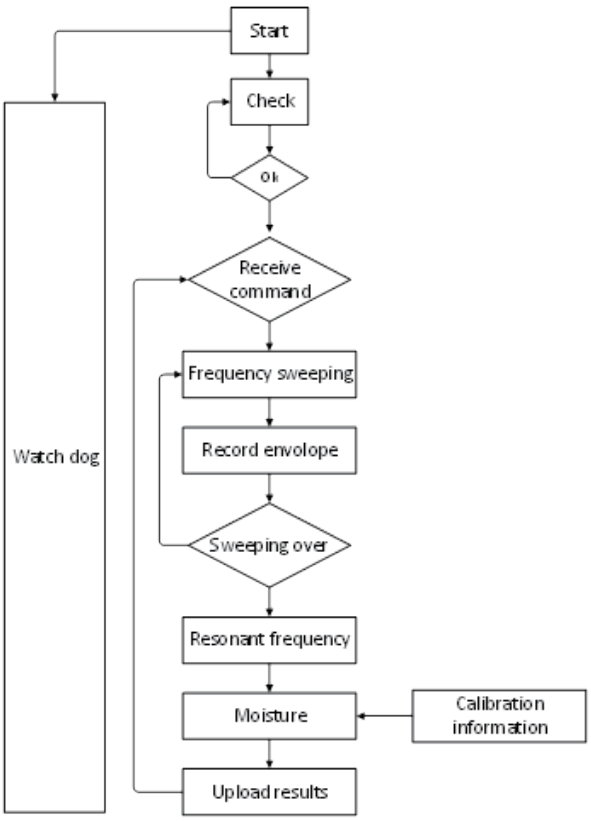

Fig. 6. Software diagram.

In this hardware check task, to validate whether DS18B20 is functional, we just read its temperature data and judge if these temperature readings are within a normal operational range (−10–70 °C). W25Q128 is validated by writing and reading a specific address and checking whether the written and read data are the same. Then, we initialize the hardware, including ADS1115, AD8317, and ADF4351. We let ADF4351 output different frequencies of around 3 GHz and check if the respective readings from ADS1115 vary accordingly. The underlying rationale is that as the Q factor of this resonant frequency is rather high, the detected envelope of AD8317 should vary. When all the hardware checks are passed, the program proceeds to the next step. If not, the program stops here.

After the hardware check, the program enters into an infinite loop where it waits for commands from the RS485 interface. There are three different commands for obtaining data: one-shot moisture sensing, periodic moisture sensing, and $S21$ parameter report. Despite the contents of these commands, the system performs the same working procedures after receiving these commands but only differs in the uploaded results. For one-shot moisture sensing, as the name refers, the system performs moisture sensing only once and then enters into an idle state. After receiving periodic moisture sensing, the results will be uploaded to a workstation repeatedly. For the $S21$ parameter report, the raw readings from the high-precision ADC will be uploaded. These raw readings may be helpful for identifying the material under test so that the system can automatically choose a corresponding calibration formula. There are other three

commands to change the parameter of the sweep frequency. Utilizing these commands, we can set the appropriate start frequency, end frequency, and precision of sweep frequency according to the actual requirements.

After receiving a valid command, the system would perform a frequency sweep. At each step, the respective ADC readings will be recorded locally. If the sweeping process is completed, a peak detection algorithm kicks in to determine the frequency corresponding to the maximum peak. This detected frequency is deemed as the resonant frequency in that specific test case. With predefined calibration information, we thus can infer the respective moisture. By checking the corresponding command types, the results would be uploaded to the workstation.

To improve the efficiency of human–computer interaction, we developed a dedicated PC shown in Fig. 7. In this dedicated PC, resonant frequency, temperature, and moisture can be obtained by clicking different function buttons. ADC data are saved locally via text files. The parameter setting module makes the sweep frequency and precision ranges more flexible for users.

3. Implementation and Performance Evaluation

We have implemented a prototype of our system. In this section, we first present some simulation results for the microwave cavity; then, we present our real-world performance evaluation results.

3.1 Simulation results for the microwave cavity

We first use FHSS to check the resonant frequency of our microwave cavity without any load. We leverage a sweeping frequency ranging from 0 Hz to as high as 6 GHz to stimulate the resonant frequency and check the respective *S*21 parameter. The *S*21 curve is shown in Fig. 8 and the corresponding three resonant frequencies are shown in Table 1.

From Fig. 8 and Table 1, we can observe that there are three resonant frequencies for the designed microwave cavity. From the *S*21 curve, we can deduce that the microwave cavity at the resonant frequency of 0.9 GHz has a higher Q factor than the other two. We then check the

Fig. 7. (Color online) Dedicated PC.

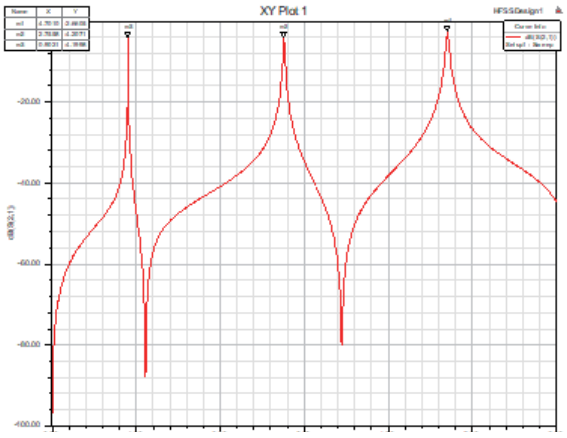

Fig. 8. (Color online) *S*21 without any load.

Table 1
Resonant frequency without any load.

p	1	2	3
Resonant frequency (GHz)	0.9021	2.7558	4.7010

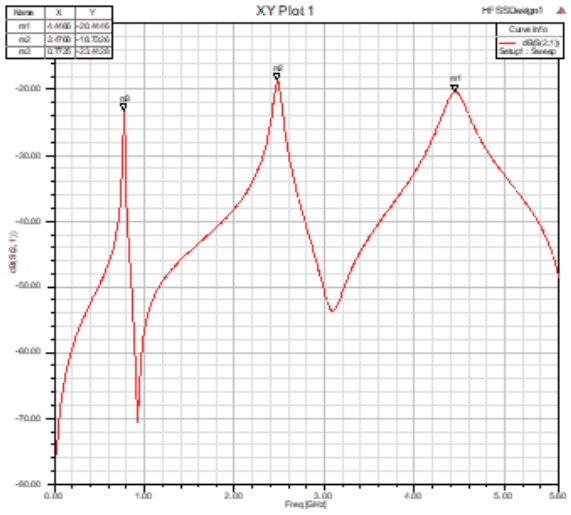

Fig. 9. (Color online) *S*21 under load of concrete (ε = 7).

Table 2
Resonant frequency under load of concrete (ε = 7).

p	1	2	3
Resonant frequency (GHz)	0.7725	2.4768	4.4466

respective behavior of this *S*21 under a load of concrete (ε = 7). The results are shown in Fig. 9 and Table 2. We can see that the three resonant frequencies change as high as up to 200 MHz. This is a notable change and hence can be readily detected by electronics.

We next change the dielectric constant ε (from 2.5 to 12) and inspect the respective resonant frequency. We aim to find a mathematical relationship between the resonant frequency and ε. The behavior of *S*21 under these dielectric constant variations can be observed from Fig. 10. At this time, it is observable that the second-order harmonic resonant frequency changes linearly under these dielectric constant variations. However, other harmonics change irregularly and hence may not be useful for our purpose. Figure 11 shows a closer look at the second-order harmonics, and Fig. 12 shows the relationship. Results reveal that the relationship between the resonant frequency and dielectric constant changes can be mathematically formulated as $f(x) = a*\exp(-b*x) + c$ (a = 0.6, b = 0.19, c = 2.31). This tells us that we can practically first check the

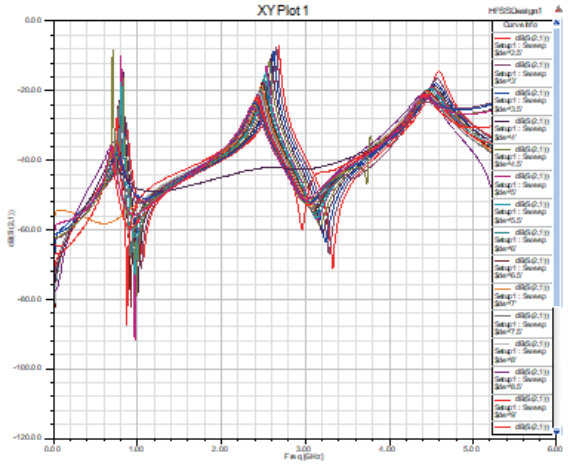

Fig. 10. (Color online) Behavior of *S*21 under different electric constants.

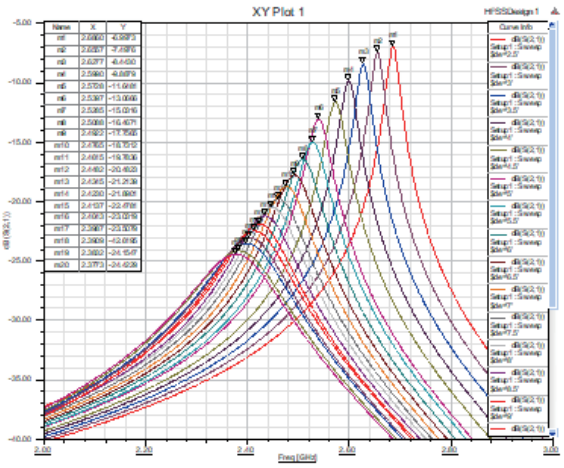

Fig. 11. (Color online) Closer look at second-order harmonics under different electric constants.

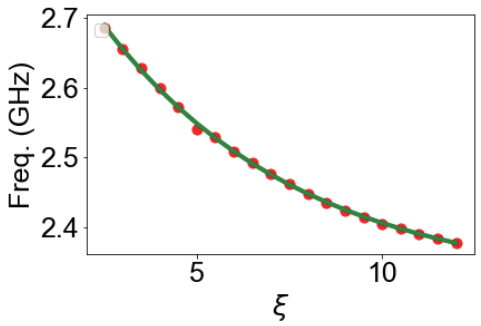

Fig. 12. (Color online) Exponential relationship between resonant frequencies under different electric constants.

resonant frequencies at three ground truth humidity levels, deducing a mathematical relationship in the off-line manner. We can then use this relationship for on-line moisture sensing.

3.2 Results for the microwave cavity in practical measurements

In this section, we present the measurement performance of a designed microwave cavity using a copper material. A snapshot of our design is shown in Fig. 13. We use a portable network analyzer LibraVNA to check the respective *S*21 parameter, and the results are shown in Fig. 14. The *S*21 curve is similar to the theoretical one, and we can observe three resonant peaks within a frequency bandwidth up to 6 GHz. However, the second-order harmonic frequency (3.2 GHz) is slightly higher than the simulated frequency (2.7 GHz). This is expected given the fabrication precision. Moreover, the excitation requires manual soldering and hence can affect the resonant

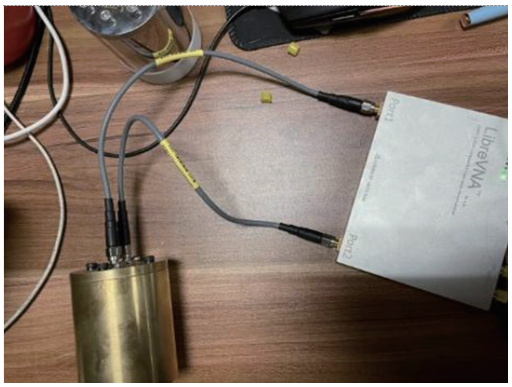

Fig. 13. (Color online) Snapshot of designed microwave cavity.

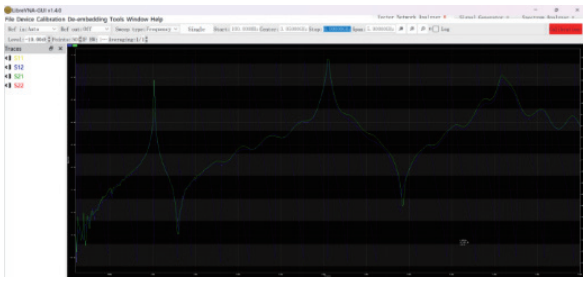

Fig. 14. (Color online) Measured *S*21 curve for our designed microwave cavity.

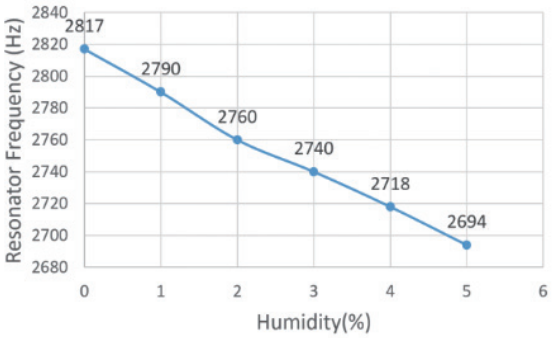

Fig. 15. (Color online) Linear relationship between resonant frequency and humidity.

frequency. Nonetheless, the waveform around the 3.2 GHz peak of the *S*21 curve is sharp, rendering the designed microwave cavity with a sufficiently high *Q*.

We next check the *S*21 curve under a brick that is made of concrete. We first heat it to 60 °C for 30 min, evaporating the water in it. We then use LibVNA to test the resonant frequency, which is around 3.1 GHz, with a deviation of 30 KHz. Then, we wet it and test *S*21 again. This time, the resonant frequency changes to 2.8 GHz, which is a change of around 300 MHz. This reveals that the designed resonator is sufficiently sensitive to humidity change.

We then use purified sand and water to obtain mixtures with ground truth humidity. We then check the respective resonant frequency. When the humidity of the mixture becomes higher than 6%, the mixture can be useless for construction; thus, the humidity in this experiment is within a percentile of 6%. A linear relationship is observed between resonant frequency and humidity, as shown in Fig. 15. This means that we practically only need to calibrate the microwave cavity sensor twice so that it can be leveraged for measurement.

3.3 Overall system performance

In this section, we present the overall system performance. At this time, we use our circuit board to retrieve the resonant frequency under measurement. Photographs of our measurements

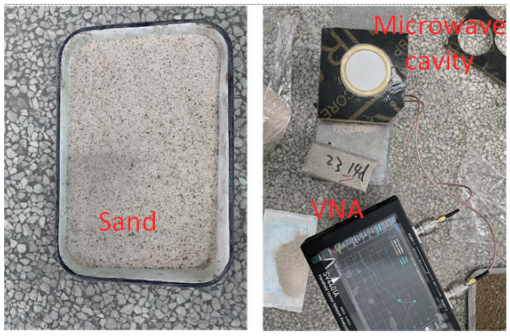

Fig. 16. (Color online) Setup.

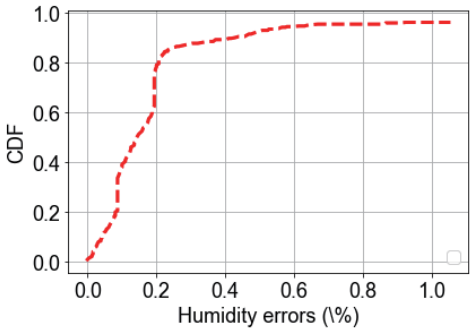

Fig. 17. (Color online) CDF of humidity measurement errors.

are shown in Fig. 16. We let our board sweep from 2.5 to 3.2 GHz with a step frequency of 10 Hz. Each sweeping frequency lasts for 2 ms. We record the respective ADC values after an envelope detector. We then calibrate the sensors for different materials with various humidity levels. The CDFs of our measurements are shown in Fig. 17. We can observe that our designed microwave cavity achieves a less than 1% humidity error, with 80% of the measurement errors being within 0.2%. The results demonstrate that our design is successful and suitable for practical measurements.

4. Conclusion

In this paper, we propose and implement a microwave cavity for sensing the moisture content of concrete for construction. We introduce an in-depth theoretical analysis behind it and design a corresponding circuit to achieve highly accurate and online moisture sensing. We have implemented a prototype and carried out extensive measurements. Results reveal that our designed microwave cavity can achieve precision as high as 1%.

Availability of Data and Materials

The datasets supporting our conclusions are included within this article.

Competing Interest

The authors declare that they have no known competing financial interests or personal relationships that could appear to influence the work reported in this paper.

References

1 M. A. W. van Ninhuijs, J. Beckers, and O. J. Luiten: New J. Phys. **24** (2022) 6. https://doi.org/10.1088/1367-2630/ac6c46
2 J. Zhou, Y. Wang, and X.-Q. Yang: IEEE Trans. Microwave Theory Tech. **7**0 (2022) 3. https://doi.org/10.1109/TMTT.2021.3129774

3 F. Chen, A. D. Warning, A. K. Datta, and X. Chen: J. Food Eng. **195** (2017) 191. https://doi.org/10.1016/j.jfoodeng.2016.09.018
4 S. N. Artemenko, S. A. Gorev, V. S. Igumnov, S. A. Novikov, and V. L. Pazynin: IEEE Trans. Microwave Theory Tech. **69** (2021) 2. https://doi.org/10.1109/TMTT.2020.3042509
5 I. C. Hunter, L. Billonet, B. Jarry, and P. Guillon: IEEE Trans. Microwave Theory Tech. **5**0 (2002) 3. https://doi.org/10.1109/22.989963
6 H. Kawabata, K.-I. Hasuike, Y. Kobayashi, and Z. Ma: Proc. 2006 IEEE European Microwave Conf. (IEEE, 2006) 388–391.
7 H. Kawabata and Y. Kobayashi: Proc. 2001 IEEE Asia-Pacific Microwave Conf. (IEEE, 2001) 102–105.
8 J. Xu, X. Luo, L. Z. Cao, and R. S. Chen: Proc. 2012 IEEE Asia Pacific Microwave Conf. (IEEE, 2012) 229–231.
9 R. R. Bonetti and A. E. Williams: IEEE Trans. Microwave Theory Tech. **35** (1987) 12. https://doi.org/10.1109/TMTT.1987.1133829
10 A. Kaczkowski and A. Milewski: IEEE Trans. Microwave Theory Tech. **28** (1980) 3. https://doi.org/10.1109/TMTT.1980.1130045
11 V. Giurgiutiu: Structural Health Monitoring with Piezoelectric Wafer Active Sensors (2014) 2nd ed.
12 H. Shi, L.Y. Wang, G. Q. Li, J. J. Yi, H. W. Liu, A. X. Zhang, and Z. Xu: J. Lightwave Technol. **41** (2023) 7. https://doi.org/10.1109/JLT.2022.3213850
13 T. Miura: Proc. 2006 IEEE MTT-S Int. Microwave Symp. Digest (IEEE, 2006) 1963–1966.
14 S. K. Thapa, R. K. Pokharel, B. Chen, T. Fukuda, and A. Barakat: Proc. 2022 IEEE/MTT-S Int. Microwave Symp. - IMS 2022 (IEEE, 2022) 560–563.
15 F. Pertl, M. Clarke, and J. Smith: J. Lightwave Technol. **3** (2011) 4. https://doi.org/10.1017/s1759078711000493
16 M. Sumedh, O. Ernst, M. Domenico, G. Sebastian, K. Sergey, and D. Andrey: Phys. Rev. Appl. **14** (2020) 4. https://doi.org/10.1103/PhysRevApplied.14.044040
17 L. Wang, Z. X. Xia, Y. J. Cheng, and Y. Fan: Proc. 2012 IEEE 10th Int. Symp. Antennas, Propagation and EM Theory (IEEE, 2012) 737–740.
18 J. Vanderlinde and D. E. Neuenschwander: Phys. Today **47** (1994) 8. https://doi.org/10.1063/1.2808611
19 T. Zhang: Maxwell's Equations in Media and Their Solution, Axiv. (2021).
20 R. E. Jacobsen, A. V. Lavrinenko, and S. Arslanagić: Appl. Sci.-Basel **9** (2019) 22. https://doi.org/10.3390/app9224848
21 J. Yuan, B. Yu, C. Yan, J. Zhang, N. Ding, and Y. Dong: Appl. Sci.-Basel **12** (2022) 826. https://doi.org/10.3390/app12020826
22 M. Zhu, W. Liu, and T. Zhang: Sci. China Phys. **51** (2008) 10. https://doi.org/10.1007/s11433-008-0158-7